

Toward a structural understanding of turbulent drag reduction: nonlinear coherent states in viscoelastic shear flows

Philip A. Stone,¹ Fabian Waleffe,² and Michael D. Graham^{1,*}

¹*Department of Chemical Engineering and Rheology Research Center*

²*Departments of Mathematics and Engineering Physics,
University of Wisconsin-Madison, Madison, WI 53706.*

(Dated: February 9, 2020)

Abstract

Nontrivial steady flow fields have recently been found that capture the main structures of the turbulent buffer layer. We study the effect of polymer on these “exact coherent states” (ECS) in plane Couette flow. When the Weissenberg number based on the largest Liapunov exponent for the velocity field is $\gtrsim 1/2$ and the polymer extensibility is sufficiently high, the Reynolds number at which the ECS appear increases from the Newtonian value. Correspondingly, wall-normal motion in the streamwise streaks is suppressed, reducing the redistribution of mean shear and leading to drag reduction.

PACS numbers: 83.60.Yz,83.80.Rs,47.20.Ky,47.27.Cn

Rheological drag reduction, the suppression by additives of skin friction in turbulent flow, has received much attention since its discovery in 1947 [1, 2, 3]. For many polymer-solvent systems, the pressure drop measured in the pipe flow of the solution can be 30 – 50% less than for the solvent alone. The central rheological feature of drag-reducing additives is their extensional behavior in solution: for dilute polymer solutions in particular the stresses arising in extensional flow can be orders of magnitude larger than those developed in a shear flow. This fact is well-recognized; nevertheless the mechanism of interaction between polymer stretching and turbulent structure is not well-understood and the goal of the present work is to attempt to shed light on this interaction.

The key structural observation from experiments and DNS of drag-reducing solutions is the modification of the buffer region near the wall [4, 5, 6, 7, 8, 9, 10]. It has long been known that the flow in this region is very structured, containing streamwise vortices that lead to streaks in the streamwise velocity [11]; these structures are thickened in both the wall-normal and spanwise directions during flow of drag reducing solutions [4, 5]. Because of its importance in the production and dissipation of turbulent energy [11], any effort to mechanistically understand rheological drag reduction should focus on this region.

To better understand the effect of the polymer on the buffer layer, we wish to study a model flow that has structures similar to those seen in this region but without the full complexities of time-dependent turbulent flows. Fortunately, a family of such model flows exists, in the recently-discovered “exact coherent states” (ECS) found by computational bifurcation analysis in plane Couette and plane Poiseuille flows [12, 13, 14, 15, 16]. These are three-dimensional, steady (in a traveling reference frame) flows that appear via saddle-node bifurcations at a Reynolds number near the transition value seen in experiments [17, 18]. The structure of the ECS captures the counter-rotating staggered streamwise vortices that dominate the structure in the buffer region. From the dynamical point of view, there is evidence that these states form a part of the dynamical skeleton of the turbulent flow: i.e., they are saddle points that underlie the strange attractor of turbulence [19]. Finally, the nonlinear self-sustaining mechanism underlying these states has been elucidated [20]. A perturbation of the base flow in the form of streamwise vortices redistributes the streamwise momentum of the flow. This redistribution creates spanwise fluctuations in the streamwise velocity, the “streaks”. The spanwise inflections in the streamwise velocity profile lead to a three-dimensional instability that develops into staggered nearly-streamwise vortices that

regenerate the streaks. Because the ECS capture the structures of the buffer region and are mechanistically well-understood, we believe that they provide an excellent simplified, yet still exact model flow for studying polymer drag reduction. The leading order effect of viscoelasticity on the ECS is therefore the focus of the present study.

To clarify how polymers behave in general flows, we briefly describe here a general result relating polymer stretch to flow kinematics. For a trajectory in a flow field, the Liapunov exponents give the Lagrangian time-averaged rate of stretch of material lines. If the largest Liapunov exponent, σ_{max} , is positive, the flow is extensional on average. In particular, for homogeneous turbulence, the expected value of σ_{max} is positive [21] and we show below that this is also the case for the ECS. Now consider the dynamics of a Hookean dumbbell model of a polymer in a flow field. The end-to-end vector \mathbf{q} of the dumbbell evolves in the flow field, \mathbf{v} , as:

$$\frac{D\mathbf{q}}{Dt} = \boldsymbol{\kappa} \cdot \mathbf{q} - \frac{1}{2\lambda} \mathbf{q} + \boldsymbol{\xi}(t), \quad (1)$$

where $\boldsymbol{\kappa} = (\nabla \mathbf{v})^T$, λ is the stress relaxation time for the dumbbell and $\boldsymbol{\xi}(t)$ is the random Brownian force. Noting that an infinitesimal material line satisfies the same expression but with λ^{-1} and $\boldsymbol{\xi}$ set to zero, it is straightforward to show that Hookean dumbbells will stretch indefinitely in a flow if and only if $\lambda\sigma_{max} \equiv We_\sigma > \frac{1}{2}$, where We_σ is a Weissenberg number based on σ_{max} . This result is a specific statement of an idea that originated with Lumley [22] (see also [23, 24, 25]). The computations below show the importance of We_σ in determining the effect of polymers on coherent structures.

We study here the effect of polymer on the exact coherent states that arise in a variant of plane Couette flow [16]. Denoting the streamwise direction as x , the wall-normal direction as y , and the spanwise, or vorticity, direction as z , we consider a flow with boundary conditions $\frac{\partial v_x}{\partial y} = 1$, $v_y = \frac{\partial v_z}{\partial y} = 0$ at $y = \pm 1$. The characteristic velocity, U , and the half-height of the channel, l , have been used to scale the velocity and positions, respectively. These “constant vorticity” boundary conditions provide an advantage over no-slip conditions in that they allow us to model only the buffer region in our domain by eliminating the viscous sublayer. (The exact coherent states found using no-slip BCs [13] show a qualitatively identical vortical structure, only offset from the wall by a small region that is the viscous sublayer.) Periodic boundary conditions are applied in the streamwise and spanwise directions. For this study, the wavelength of the structures in the streamwise and spanwise directions are fixed at

$\ell_x = 2\pi/0.40$ and $\ell_z = 2\pi/1.0$, respectively. For this flow, a trivial (Couette) base state exists, $v_x(y) = y$; the maximum mean velocity for the ECS is significantly reduced compared to the base state velocity due to the enhanced transport of momentum [16].

In our formulation, time, t , is scaled with l/U , and pressure, p , with ρU^2 , where ρ is the fluid density. The stress due to the polymer, $\boldsymbol{\tau}_p$, is nondimensionalized with the polymer elastic modulus, $G = \eta_p/\lambda$, where η_p is the polymer contribution to the zero-shear viscosity and λ is the relaxation time for the polymer — the polymer model is described below. The momentum balance and the equation of continuity are

$$\frac{D\mathbf{v}}{Dt} = -\nabla p + \beta \frac{1}{Re} \nabla^2 \mathbf{v} + (1 - \beta) \frac{1}{Re^2} \frac{1}{El} (\nabla \cdot \boldsymbol{\tau}_p) \quad (2)$$

$$\nabla \cdot \mathbf{v} = 0, \quad (3)$$

where η_s is the solvent viscosity, $El = \lambda(\eta_s + \eta_p)/\rho l^2$ and $\beta = \eta_s/(\eta_s + \eta_p)$. The Reynolds number, Re , is based on the total viscosity, $Re = \rho U l / (\eta_s + \eta_p)$.

We calculate the polymer stress with the commonly used FENE-P model [26], which idealizes the polymer molecules as bead-spring dumbbells with finitely extensible springs. With this model, the non-dimensional structure tensor $\boldsymbol{\alpha}$ evolves according to:

$$\frac{\boldsymbol{\alpha}}{1 - \frac{tr\boldsymbol{\alpha}}{b}} + We \left(\frac{D\boldsymbol{\alpha}}{Dt} - \boldsymbol{\alpha} \cdot \nabla \mathbf{v} - \nabla \mathbf{v}^T \cdot \boldsymbol{\alpha} \right) = \frac{b\boldsymbol{\delta}}{b+2}, \quad (4)$$

$$\boldsymbol{\tau}_p = \frac{b+5}{b} \left(\frac{\boldsymbol{\alpha}}{1 - \frac{tr\boldsymbol{\alpha}}{b}} - \left(1 - \frac{2}{b+2} \right) \boldsymbol{\delta} \right), \quad (5)$$

where $We = \frac{\lambda U}{l}$ is the Weissenberg number based on the wall shear rate and b is proportional to the maximum extension of the dumbbell: $tr\boldsymbol{\alpha}$ cannot exceed b .

A simple measure of the importance of extensional polymer stress is the magnitude of the parameter $Ex = \frac{2}{3} \frac{b\eta_p}{\eta_s}$. In uniaxial extension with extension rate $\dot{\varepsilon}$, $Ex = 1$ implies that $\boldsymbol{\tau}_p = \boldsymbol{\tau}_v$ as $\dot{\varepsilon} \rightarrow \infty$ where $\boldsymbol{\tau}_v$ is the solvent contribution to the stress. The polymer can significantly affect the flow only when $Ex \gtrsim 1$.

The governing equations are solved through a Picard iteration. A given velocity field is first used to calculate the polymer stress tensor, $\boldsymbol{\tau}_p$, by time-integrating Eq. 4 until a steady state is attained. For the new $\boldsymbol{\tau}_p$, a steady state of the momentum and continuity equations is found by Newton iteration. The resulting velocity field, is used to compute the new $\boldsymbol{\tau}_p$, and the process is repeated until the velocity field converges. The procedure converges at $El = 0.2$ for values of Ex up to about 2, sufficient to show the first effects of polymers

on turbulent structure. The momentum and continuity equations are discretized as in [16], using a Fourier-Galerkin formulation with typically a $7 \times 19 \times 7$ grid. The structure tensor, α , is discretized with a Fourier-pseudospectral method and time-integration performed with an Adams-Bashforth method. To achieve numerical stability, a small diffusive term is added to Eq. 4 (cf. [9]) and integrated with a Crank-Nicholson scheme. This equation was solved on a finer mesh than the momentum, continuity pair, typically $32 \times 32 \times 32$.

Before presenting the effects of the polymer on the ECS, we recall the result that $We_\sigma > 1/2$ implies large stretch of polymer chains. We have computed σ_{max} with the algorithm of [27] for the Newtonian ECS velocity field at $Re = 110$ on the upper branch of the bifurcation diagram (see Fig. 1). This vector field is very nearly ergodic, with $\sigma_{max} \approx 0.030$. The condition $We_\sigma > 1/2$ thus translates into $We \gtrsim 17$ for large polymer stretch, and for $Ex = O(1)$, will define the onset condition for the polymer to begin to strongly affect the flow field. In DNS of a FENE-P fluid in plane channel flow, Sureshkumar, et al. [9], found no drag reduction at $We = 12.5$ and significant drag reduction at $We = 25$. This close correspondence between the onset condition predicted from the ECS kinematics and that found by DNS suggests that the ECS model captures the essential structure of the buffer layer.

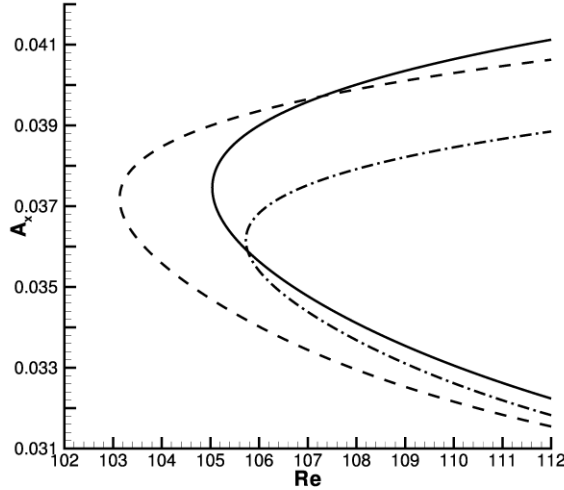


FIG. 1: Newtonian and viscoelastic ($El = 0.20$, $\beta = 0.97$) bifurcation diagrams. — Newtonian; — — — $Ex = 1$; — · — $Ex = 2$.

Fig. 1 shows how the addition of polymer stress affects the bifurcation diagram for $El =$

0.20 (where $We_\sigma \approx 2/3$) and $Ex = 1$ and 2. On the y -axis of the diagram is the variable A_x , which is the amplitude of the velocity mode corresponding to the wavevector $\mathbf{k} = (1, 0, 0)$. Hence, A_x is a measure of the streamwise “waviness” in the streamwise streak and provides a simple measure of the three-dimensionality of the flow. The Couette flow solution is the line $A_x = 0$. When Re attains a certain value that we denote Re_{sn} , two new solutions appear in a saddle-node bifurcation. For sufficiently high values of the extensibility parameter ($Ex \approx 1.5$) Re_{sn} increases above the Newtonian value – the presence of the polymer is suppressing the ECS. For lower values of Ex , where the polymer stress is smaller in relation to the viscous stress, Re_{sn} decreases compared to the Newtonian value. A minimum in Re_{sn} is also seen when varying the elasticity at constant extensibility.

To examine more closely the effect of the polymer stress on the three-dimensionality of the solutions, Fig. 2 shows results at constant Re while varying El , or, equivalently, We_σ (based on the Newtonian value $\sigma_{max} = 0.030$ found at $Re = 110$). After an initial increase in the three-dimensionality for $El = 1$, A_x decreases below the Newtonian value and eventually saturates, as the polymer stress asymptotes at high We_σ to a fixed value relative to the viscous stress. In this case, the polymer stretch becomes nearly uniformly large throughout the domain. The decrease in A_x with We_σ is even more drastic as the extensibility parameter increases from $Ex = 1$ to $Ex = 2$. Identical trends are seen for the spatially averaged streamwise enstrophy, consistent with DNS results [10]. Since Ex is related to the extensional viscosity of the viscoelastic solution, these results show the importance of extensional stresses in affecting the ECS. The maximum over the domain of $tr\alpha$, which is proportional to the square of the polymer extension is also presented in Fig. 2. Most of the polymer stretch occurs for $We_\sigma \lesssim 1.0$. This figure also reemphasizes the importance of We_σ in determining the effect of polymer on flow. The majority of both the polymer stretch and the suppression of the three-dimensionality occurs in the range $0.1 < We_\sigma < 1.0$.

Figs. 3a-b show (a) the streamwise velocity v_x at $y = 1$ for the Newtonian upper branch solution at $Re = 110$ and (b) the difference $v_{x,VE} - v_{x,N}$ between the viscoelastic (VE) and Newtonian (N) solutions. In this figure we see the “streak” (white ribbon) and that this streak is “straightened out” by the viscoelasticity. Plots of surfaces of constant streamwise velocity and constant polymer extension (Fig. 4) show that the highest polymer stretch (which is predominantly in the streamwise direction) corresponds to the streaks in the

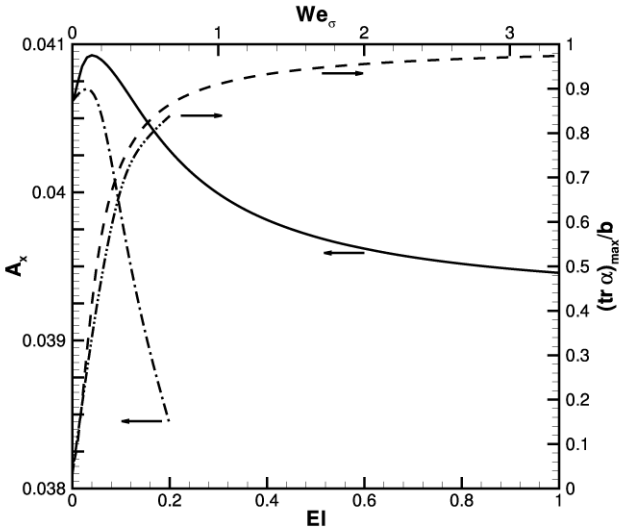


FIG. 2: Three-dimensionality and maximum polymer stretch *vs.* El and We_σ , upper branch solutions, $Re = 110$, $\beta = 0.97$. Three-dimensionality: — $Ex = 1$; — · — $Ex = 2$; Extension: — — — $Ex = 1$; — · · — $Ex = 2$.

streamwise velocity. Very little stretch is seen in the cores of the vortices, an observation which does not support proposed mechanisms of drag reduction based on suppression of vortex stretching, e.g. [28]. Based on the above observations, we believe that the elongation of the polymer in the streamwise streak alters the ECS by a streamline tension mechanism [29, 30, 31]. The extra tension in the streaks causes them to resist spanwise deformation, weakening the effect of the inflectional instability that feeds the vortices and thereby suppressing the redistribution of momentum. This effect is also seen in the wall-normal velocity, whose maximum value (under the same conditions as in Figs. 3 and 4) is reduced from the Newtonian value by 5.9%.

Finally, do we see drag reduction? This question can be addressed in two ways. First, consider Fig. 1. For the Newtonian flow, $Re_{sn} \approx 105$. For $El = 0.2$ and $Ex = 2$, $Re_{sn} \approx 106$. The existence of the ECS, which, of course, have higher drag or, in the present situation, lower maximum velocity for a given wall shear rate than the Couette solution, is shifted up in Re . This is a small change, but here We_σ and Ex are just on the edge of where polymer stress can compete with viscous stress. Furthermore, drag reduction can be directly seen in the streamwise velocities, the maximum value of which increases from the Newtonian value for sufficiently high Ex and We_σ , as seen in Fig. 3.

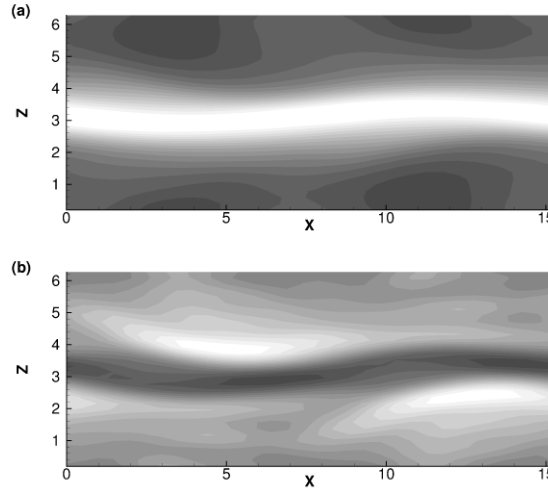


FIG. 3: Streamwise velocity for the Newtonian(N) and viscoelastic(VE) upper branch solutions $Re = 110$ and $y = 1$. (a) $v_{x,N}$ (range: 0.0 (black) — 0.889 (white)) (b) $v_{x,VE} - v_{x,N}$ (range: -0.0196 (black) — 0.0196 (white)); for the viscoelastic solution $El = 0.15$, $Ex = 2$, and $\beta = 0.97$.

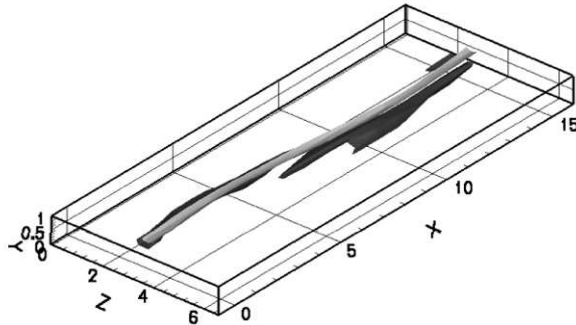


FIG. 4: Polymer stretch and streamwise velocity in upper half of domain. Light gray surface is constant v_x at 95% of $v_{x,max}$. Dark gray surface is constant polymer stretch, $tr\alpha = 0.93(tr\alpha)_{max}$ ($El = 0.15$, $Ex = 2$, $\beta = 0.97$).

Although the results have begun to reveal the structural mechanisms of drag reduction, many questions remain. Most importantly, the relation between the largest Liapunov exponent and the turbulent structure must be explored further. In particular, we expect that wider, thicker streamwise vortices are less effective than narrow, thin ones at stretching material elements, thus explaining the observed shift toward these larger scale structures in flows of drag-reducing fluids. Also, further work is needed on the dynamical relationship between the ECS and the coherent structures of turbulence, including broader studies, probing

higher values of Ex and Re , of the effects of polymer on the bifurcation structure of wall-bounded shear flows. This will require abandoning the Picard iteration for a full Newton iteration for a non-symmetric system with $O(10^6)$ unknowns. Finally, given that the ECS provide a well-controlled model of boundary layer turbulence, they can be effectively used to probe the effects of other rheologically complex drag-reducing fluids such as fiber and surfactant solutions, ultimately leading to a firm understanding of the interaction between rheology and turbulence.

* Electronic address: graham@engr.wisc.edu

- [1] P. Virk, *AIChE J.* **21**, 225 (1975).
- [2] J. Lumley, *Annu. Rev. Fluid Mech.* **1**, 367 (1969).
- [3] W. McComb, *The Physics of Fluid Turbulence* (Oxford University Press, New York, 1990).
- [4] D. Walker and W. Tiederman, *J. Fluid Mech.* **218**, 377 (1990).
- [5] G. Donohue, W. Tiederman, and M. Reischman, *J. Fluid Mech.* **50**, 559 (1972).
- [6] J. den Toonder, M. Hulsen, G. Kuiken, and F. Nieuwstadt, *J. Fluid Mech.* **337**, 193 (1997).
- [7] A. Draad, G. Kuiken, and F. Nieuwstadt, *J. Fluid Mech.* **377**, 267 (1998).
- [8] M. Escudier, F. Presti, and S. Smith, *J. Non-Newtonian Fluid Mech.* **81**, 197 (1999).
- [9] R. Sureshkumar, A. Beris, and R. Handler, *Phys. Fluids* **9**, 743 (1997).
- [10] C. Dimitropoulos, R. Sureshkumar, A. Beris, and R. Handler, *Phys. Fluids* **13**, 1016 (2001).
- [11] S. Robinson, *Annu. Rev. Fluid Mech.* **23**, 601 (1991).
- [12] B. Eckhardt, K. Marzinzik, and A. Schmiegel, in *A Perspective Look at Nonlinear Media* (Springer, New York, 1998), Lecture Notes in Physics.
- [13] F. Waleffe, *J. Fluid Mech.* **435**, 93 (2001).
- [14] M. Nagata, *J. Fluid Mech.* **217**, 519 (1990).
- [15] R. Clever and F. Busse, *J. Fluid Mech.* **344**, 137 (1997).
- [16] F. Waleffe, *Phys. Rev. Lett.* **81**, 4140 (1998).
- [17] F. Daviaud, J. Hegseth, and P. Bergé, *Phys. Rev. Lett.* **69**, 2511 (1992).
- [18] S. Bottin, O. Dauchot, F. Daviaud, and P. Mannveille, *Phys. Fluids* **10**, 2597 (1998).
- [19] J. Jimenez and M. Simens, *J. Fluid Mech.* **435**, 81 (2001).
- [20] F. Waleffe, *Phys. Fluids* **9**, 883 (1997).

- [21] S. Girimaji and S. Pope, *J. Fluid Mech.* **220**, 427 (1990).
- [22] J. Lumley, *Symp. Math.* **9**, 315 (1972).
- [23] L. G. Leal, in *Structure of Turbulence and Drag Reduction* (Springer-Verlag, 1990).
- [24] M. Chertkov, *Phys. Rev. Lett.* **84**, 4761 (2000).
- [25] E. Balkovsky, A. Fouxon, and V. Lebedev, *Phys. Rev. Lett.* **84**, 4765 (2000).
- [26] R. Bird, C. Curtiss, R. Armstrong, and O. Hassager, *Dynamics of Polymeric Liquids*, vol. 2 (Wiley, New York, 1987), 2nd ed.
- [27] G. Benettin, L. Galgani, and J. Strelcyn, *Phys. Rev. A* **14**, 2338 (1976).
- [28] A. Yarin, *J. Non-Newtonian Fluid Mech.* **69**, 137 (1997).
- [29] J. Azaiez and G. Homsy, *J. Fluid Mech.* **268**, 37 (1994).
- [30] J. Rallison and E. Hinch, *J. Fluid Mech.* **288**, 311 (1995).
- [31] M. Graham, *J. Fluid Mech.* **360**, 341 (1998).